

Electrical and Optical Properties, for Nano $(\text{SiO}_2)_{100-x} : (\text{NiO})_x$ Glassy Matrix.

M. El-Shaarawy^a, M. Abd EL-rafa^b, M. Gouda^a, H. Khoder^a, Mervat .Ramadan^c

^aPhysics Department, Faculty of Science, Banha University

^bAdvanced Technology and New Materials Institute, for Scientific Research and Technology Applications Borg El Arab City, Alexandria,

^cPhysics Department, Faculty of Science and Arts onayza ,Qassim University.

Abstract: Nickel Oxide doped silica glass with nominal composition $(\text{SiO}_2)_{1-x} : (\text{NiO})_x$ (mol%) is prepared using the sol-gel method. and characterized by various analytical technique. The structure has been examined using X-ray diffraction (XRD) and show average grain size of the NiO nanoparticles 5.55 nm to 9.04. Fourier transform infrared spectroscopy (FT-IR), scanning electronic microscopy (SEM). Transmission electron(TEM) average nanoparticles size (1.44–7.92 nm). . Measurements of the a.c. conductivities and dielectric constant, with frequency, respectively, for nano glasses: $(\text{SiO}_2)_{1-x} : (\text{NiO})_x$ have been made on the glassy system, , in the temperature range 300-500 K and in the frequency range 100 Hz to 100 kHz. we have found. The a.c. conductivity increase with increase frequency .UV-visible measurements found the optical band gap (E_g) approx 0.49 ev. The coercivity values H_c ,the magnetization M_s and the remanence values M_r and the reduced remanence M_r/M_s obtained from the hysteresis loops From these data, it was found that the saturation magnetization for NiO increases, while the coercive field values decrease, by increasing NiO content.

Key words: Nanocomposite , nickel oxide, optical properties, dielectric

I. Introduction

Sol-gel technique has been used extensively to prepare novel ceramics or glass materials. One of the applications of this technique is to fabricate glass-metal nano-composites [1]. Nanocomposites are important

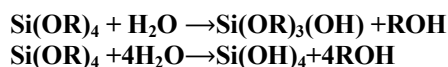
class of materials because of many of their physical and chemical properties show particle size dependence [2-5]. Nanstructured metal (Zn, Mg, Ca) structure, dispersed in SiO_2 glassy matrix materials are found to exhibit improved properties such as great thermal stability, hardness, etc. and thus, gained interesting importance in the technological applications like optical, refractories, high alumina cement oxidation catalysts, electronic and optoelectronic applications [6]. Nanoparticles and nanomaterials represent an evolving domain of research with a strong impact on an incredibly wide number of industries and markets. Many novel properties and applications of nanoparticles have already been demonstrated in domains as catalysis, environmental remediation, biomedicine, information technology and/or electronics[7]. The metal

Nan composite materials can be obtained by controlling both the size and polydispersity of the particles in the host matrix through various synthesis methods, under specific conditions, like sol-gel, solid state reaction, etc. [8]. Wide varieties of glass, glass-ceramic monoliths, nano-structured powders, etc. are synthesized through sol-gel technique, since it has many advantages over other methods like low temperature processing, high chemical homogeneity, and purity, etc. Hence, the above mentioned advantages focused our attention to synthesize a nanocrystals of spinel structured NiO dispersed in SiO_2 glassy matrix through sol-gel reaction and characterize by XRD, FTIR. One of the most studied sol- gel system is $\text{Fe}_x\text{O}_y - \text{SiO}_2$ [9]. Nanocomposites belonging to the mentioned system have a great importance due to their specific properties and hence due to their application in domains as catalysis ,medicine, magnetic media. The SiO_2 source for preparing $\text{Fe}_x\text{O}_y - \text{SiO}_2$ nanocomposite systems is mainly an alkoxide: triethoxysilane [10], nanoparticles, Ni in particular, are attractive. Due to their interesting physical properties, nanocomposites formed by nickel and nickel oxide embedded in a silica matrix obtained by sol-gel have been widely studied using diverse methods with different precursor compounds [11–16]. However, the optical properties of Ni nanoparticles are studied rather poorly. We have found a few works reporting results of optical study of nickel nanoparticles in sol-gel fabricated silica film . Depending on the processing parameters, nickel was found in different chemical states, that is, as Ni^{+2} ions, nanoparticles of nickel oxide and metallic nickel dispersed in the SiO_2 matrix. Each species produces characteristic features in the optical spectra.

II. Experimental

Nano glassy samples were prepared by the sol-gel technique .The starting sol was obtained by mixing tetraethyl orthosilicate (TEOS) (Aldrich, 99%), an (Ethanol, 98%), water and nickel nitrate $\text{Ni}(\text{NO}_3)_2 \cdot 6\text{H}_2\text{O}$ [Aldrich, 98%] TEOS: $\text{C}_2\text{H}_5\text{OH}:\text{H}_2\text{O}:\text{Ni}(\text{NO}_3)_2 \cdot 6\text{H}_2\text{O}$, molar ratio of 1: 3: 1: x, where x is (0.05),(0.10),

(0.15), (0.20), (0.25) and (0.30)) of the Nickel Oxide concentration in the dried glass ,following the procedure reported in ref[7, 13, 17] The chemical reactions occurred throughout the bulk of the matrix are as Follows, The most common studied metal alkoxides is silicon tetraethyl orthosilicate (TEOS; Si(OC₂H₅)₄). The TEOS precursor can react readily with water via the following reaction[18]:



Subsequent condensation reaction sequences produce cluster species with Si–O–Si (siloxane) bonds and water or alcohol as the by-products:



(R= CH₂CH₃)

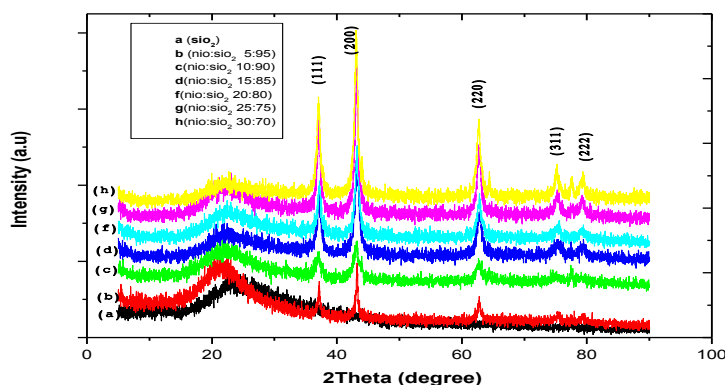
X-ray diffraction patterns (XRD) of the samples powder using diffractometer of type “Schimadzu 7000 maxima”. The measurements were done within the angular range 2θ = 10°-100° and scanning rate 2 degree/min. A target of CuKα1(λ=1.5406). FT-IR spectra for nano glasses were recorded using spectrophotometer model (Shimadzu 8400S) The powder morphology and homogeneity were imaged and measured by SEM of type "Jeol-JSM-636 OLA" with EDX .analysis EDX is a technique used for identifying the elemental composition of the specimen, or an area of interest thereof. The EDX analysis system works as an integrated accessory of a scanning . transmission electron microscope(TEM 100 CX) characterization for sample . Dielectric and electrical measurements were carried out in the temperature range 303–473K using PM 6304 programmable automatic RCL (Philips) meter. The measurements were carried out over a frequency range 100 Hz to 100 kHz. ViS spectrometer PG instruments Ltd) was used to study samples as solution . /UV-Spectrometer (T80 + UV The three groups samples were analyzed by the UV-Spectroscope It uses light in the visible and ultra violet ranges. Magnetic measurements the saturation magnetization (Ms), remnant magnetization (Mr) and coercivity (Hc) will be studied by measuring the hysteresis loops.

III. Result and discussion

3.1.Characterization

3.1.1.X-Ray Diffraction

The XRD patterns of the nanocomposite (SiO₂)_{1-x}:(NiO)_x where x =0,5,10,15,20,25and 30 have been shown in fig.(1). The patterns shown maxed phase with well crystallized NiO spread on amorphous SiO₂. From this figure we observed a bread signal at about 2θ = 22° for all samples which is due to the SiO₂ vitreous matrix [19]. In addition, strong Si(111) peak at 37.2° was observed .the intensity of this peak increases with increasing the concentration of nickel oxide .on the other hand ,the patterns of (SiO₂ : NiO) nanocomposite



Fig(1) . XRD spectra for (SiO₂ :NiO) sample heat temperature at 673k for 4h and molar ratio(a) 0:100 (b) 5:95 (c)10:90 (d)15:85(f) 20:80 (g) 25:75 (h) 30:70 .

Display representative NiO peaks centered at 2θ=43.06° , 62.72° ,75.48° and79.26° corresponding to(200),(220),(211) and (222) planes respectively .Since the relative intensity of the NiO(200) diffraction peaks ,compared to the (111) and (220) peaks, increases gradually by increasing nickel oxide concentration. So ,we suggested that the NiO (200) diffraction peak dominates in the present work .

The average size of the particles can be calculated by the Scherrer Formula[20].

$$d = \frac{0.9\lambda}{\beta \cos \theta} \quad (1)$$

Where *d* is the average size of the particle, λ is the wavelength of the X-ray. β is the full width at half maximum (FWHM) of the diffraction peak, and θ is the corresponding diffraction angle of the diffraction peak. According to the data in Fig. 1. and formula (1), the average particle size of the nano-Nio (4.6-9.04 nm) .

Table(1) Average particle size for all sample.

Nio content wt%	Average particle size (nm) by Scherrer equation	Average particle size (nm) byTME
5	5.55	
10	9.04	3.098
15	4.56	
20	4.89	3.392
25	6.63	
30	5.51	1.760

3.1.2. Fourier-Transform-Infrared Spectrometry (FTIR)

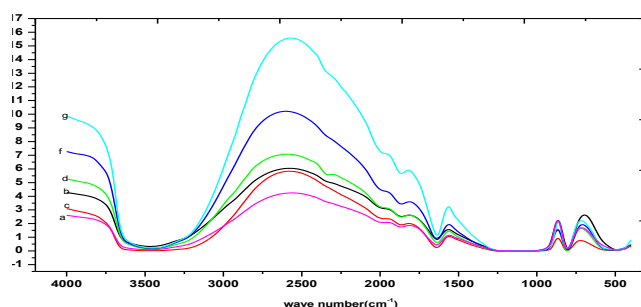


Fig. 2. IR spectra for sample (SiO₂:NiO:) (a) 95: 5 ,(b)90:10,(c)85:15.(d)80:10,(f)75:25,(g)70:30 thermally treated at 673 k° for 4 h ,and at 1173k° for 1 h

Fig.2. shows the FTIR spectra of the sample, the broad bands in the regions of 3473.65 – 3460.06 cm⁻¹ and 1978.83 – 1866.97 cm⁻¹ and at 1637.45 cm⁻¹ may be attributed respectively to stretching and bending vibrational modes of O-H of molecular water and the Si-OH stretching of surface silanol hydrogen bond to molecular water. The band at 1151.42 cm⁻¹ and 806.19 cm⁻¹ may correspond to the presence of nitrate groups. The bands at 1091.63, 1054.99 and 464.81cm⁻¹ are attribute to the stretching and bending vibrations of Si-O-Si bonds. showed the disappearance of band positions of 3465, 1640, 1376 and 816 cm⁻¹. The broad band at 1080.06- 1031.85 cm⁻¹ may be due to stretching mode of broken Si-O- bridges [6]. The band at 482.17 cm⁻¹ corresponds to the deformation mode of Si-O-Si. The broad absorption band in the region of 600–700 cm⁻¹ is assigned to Ni–O stretching vibration mode cm⁻¹ which is attributed to the Ni-O vibration is also present in all the studied spectra, hence, the IR data prove the presence of Nickel Oxide in the silica matrix[7]. note increase the proportion of nickel oxide in relation to silica oxide increases the absorption FTIR and note agree with the results of the absorption XRY.

Table(2) FT-IR absorption bands positions for all samples

Vibration frequency(cm ⁻¹)	bands	Nio content wt%					
		5%	10%	15%	20%	25%	30%
3500-3300	O-H stretching	3473.58	3465.84	3465.8	3454.27	3454.27	3452.34
1640-1560	N-H bending Broad band	1637.45	1639.38	1639.38	1637.45	1637.45	1635.32
1120-820	symmetric stretching vibration nitrate groups (No) ₃	806.19	802.3	806.19	806.19	802.33	804.26
1330-1000	bending and asymmetric stretching vibrations of Si-O-Si and Si-OH	1151.1.42	1228.28	1242.07	1238.2	1230.5	1232.4
1240-975	stretching mode of broken Si-O- bridges	1054.9	1211.2	1147.27	1153.35	1097.4	1176.5

700-600	Ni-O-Ni stretching vibration mode	686.3	673.6	680.8	692.39	676.6	687.89
---------	-----------------------------------	-------	-------	-------	--------	-------	--------

3.1.3 .Scanning Electron Microscope (SEM) and analysis (EDX)

In fig.3.The SEM and EDAX image of (SiO₂ :NiO) particles has been shown The particles seem to be bigger in size and in aggregated form. EDAX results suggest the presence of Si and oxygen elements, confirming the formation of sio₂ particles. The morphology of the Nio nanoparticles is examined by SEM (Fig. 3). From the micrograph, it was observed that the nanoparticles were semi-spherical.

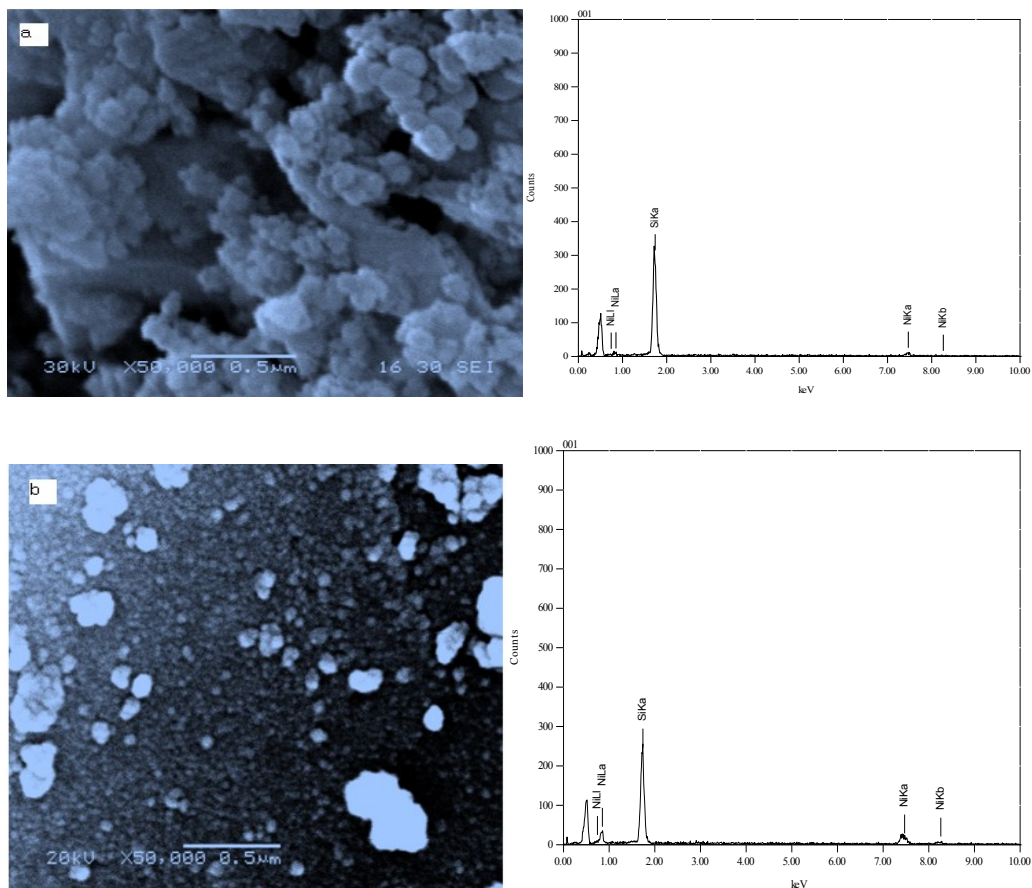


Fig.3. SEM micrographs for nanostructure(SiO₂: NiO) (a) 90:10 ,(b)(85:15) annealed in air for 673k^o for 4h and at1173k^o for 1 h.

3.1.4. Transmission Electron Microscope (TEM)

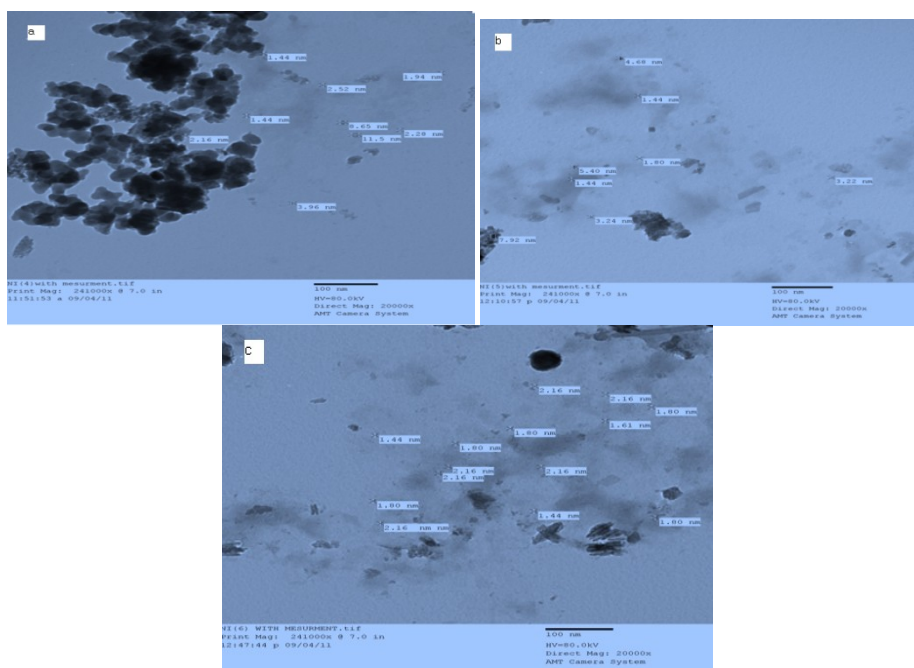


Fig. 4. TEM micrographs for nano structured $(\text{SiO}_2:\text{NiO})$ (a) 90:10, (b) 80:20, (c) 70:30 annealed in air for sample temperature at 673k° for 4h and at 1173k° for 1 h,

TEM image (Fig. 4) shows the presence of dense agglomerates. The particles have a spherical shape, and their distribution, likewise, is not uniform and crystals are dispersed in the SiO_2 -based glass and the crystalline size is in the range of (1.44 – 7.9) nm.

3.2. 1. The a.c. conductivity as a function of frequency

Fig.5. The frequency dependent on a.c. conductivity at different temperatures $(\text{SiO}_2)_{100-x}:(\text{NiO})_x$ where $x=10\%$, 25% . We have performed the measurement of ac conductivity of $(\text{SiO}_2:\text{NiO})$ nano having different NiO concentration in the frequency range 100 Hz to 100 KHz. plot shows the frequency independent plateau region at low frequencies and a dispersive region at high frequencies, the frequency exponent s is less than 1. From this figure, it is seen that the a.c. conductivity increases with increasing frequency for all samples on different isotherms. From the measurements of the variation of the a-c. conductivity with frequency at different temperatures the value of the frequency exponent s , the slope of the linear dependence of $\log \sigma$ versus $\log \omega$, has been measured. The numerical values of s at room temperature are in the range $0.33 < s < 0.71$, which are closely associated with proven carrier transport: hopping electrons. frequency dependent ac conductivity due to the hopping conduction charge [21]. According to the Jonscher, the frequency dependence part ($\sigma(\omega)$) i.e. the ac conductivity is caused by the mobile charge carriers. As the mobile charge carriers hops to a new site, from its original position, it faces some displacements between the two minimum potential energy states. can be analyzed by the power law exponent.

$$\sigma = A\omega^s \quad (2)$$

where A is the temperature-dependent constant and the frequency exponent s is less than 1.

Generally, the electrical conductivity directly related to the amount of free or bond charge carriers as well as to their mobility. The ionic conduction of the samples results from the migration of exchangeable the channels and cavities of the grains according to an ion-hopping mechanism.

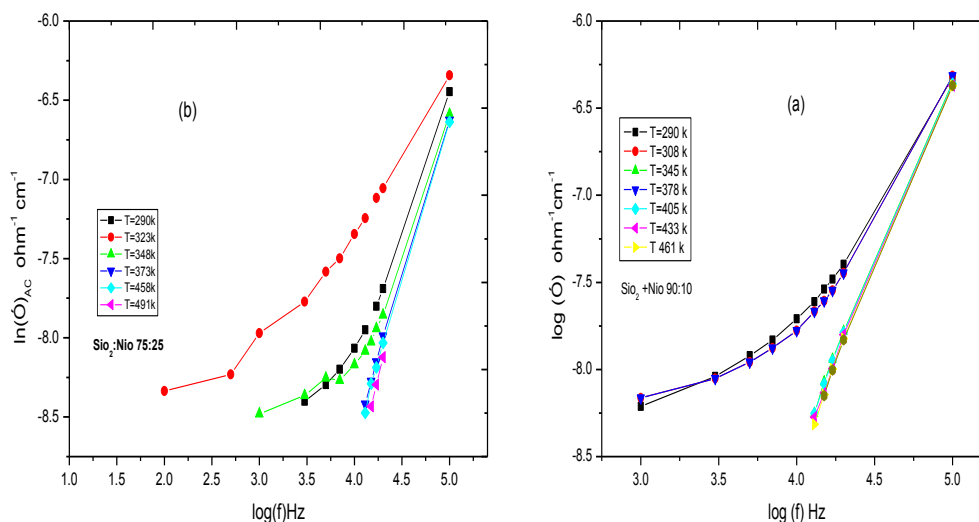


Fig. 5. The frequency dependent conductivity at different temperatures for nano glasses ($\text{SiO}_2:\text{NiO}$)(90:10),(75:25).

3.2.2. The dielectric constant

The frequency dependent measurements of capacitance, C, for different frequencies in the range 100 Hz to 100 kHz and temperature from 300 to 500 K. The dielectric constant, determined as the following

where ϵ_0 is the permittivity of free space, d is thickness of the nano glass sample and A is cross sectional area of the sample.

Fig. 6.(a). The dielectric constant for nano samples $(\text{SiO}_2)_{100-x}:(\text{NiO})_x$ where $x=5\%$, are found to decrease with increase of frequency and saturates at higher frequencies. It is evident that single power function does not explain the observed decrease in the dielectric constant. The high value of dielectric constant at low frequencies is attributed to the interfacial ionic polarizations due to localized (no) ion motion within the sample. The experimental results obtained in the present study for shows the frequency dependence of the dielectric constant, for the sample at different temperatures dielectric permittivity can be explained by Stevel's model on dielectric relaxation in glass[22]. crystalline materials consist of grain or interface boundaries. These boundaries contain defects such as dangling bonds, vacancies, clusters etc. These defects can cause a positive or negative space charge distribution at interfaces. The space charge can move on the application of an external field and when they are trapped by the defects lot of dipole moments were formed This is the space charge polarization. Hence the space charge effect will be a prominent factor, which decides the dielectric properties in materials with small particle sizes. In addition ion jump polarization may also be greater in nano crystalline materials since there will be a number of positions in the grain boundaries for the ions to occupy. The high values of the dielectric constant in the present study may be attributed to the increased ion jump orientation effect and the increased space charge effect exhibited by nanoparticles, the charge carriers tend to pile up at high free energy barriers resulting in an increase of capacitance at low frequency. Thus, the variation of dielectric constant at lower frequencies is due to the long range diffusion of Ni ions involving series of jumps over barriers of varying height. At higher frequencies, the periodic reversal of field takes place so rapidly that there are no excess ionic jumps in the field direction[23]. The capacitive effect at the high free energy barrier site disappears at high frequencies and results in the low value of dielectric constant as shown in Fig.6.(a). and It is seen that the dielectric constant of the samples is much lower and also there is no much variation with temperature at high frequencies. But at low frequencies the variation is high. The rest of the samples behave the same behavior representative In fig. 6.(b). the temperature dependencies of dielectric constant at different constant frequencies for samples of system $(\text{SiO}_2)_{100-x}:(\text{NiO})_x$ where $x=5\%$ these curves show that the dielectric constant for all sample generally decrease as the temperature increases

The variations of dielectric constant with temperature for nano SiO₂)_{100-x}:(NiO)_x is shown in Fig .6.b. It is seen that the dielectric constant of the sample is much lower and also there is no much variation with temperature at high frequencies. But at low frequencies the variation is high. A large volume percentage of crystalline materials consist of grain or interface boundaries. These boundaries contain defects such as dangling bonds, vacancies,. These defects can cause a positive or negative space charge distribution at interfaces .The space charge can move on the application of an external field and when they are trapped by the defects lot of dipole moments were formed. field and when they are trapped by the defects lot of dipole moments were formed [24].

This is the space charge polarization. Hence the space charge effect will be a prominent factor, which decides the dielectric properties in materials with small particle sizes. In addition ion jump polarization may also be greater in nanocrystalline materials since there will be a number of positions in the grain boundaries for the ions to occupy. The high values of the dielectric constant in the present study may be attributed to the increased ion jump orientation effect and the increased space charge effect exhibited by nanoparticles. Most of the atoms in the nanocrystalline materials reside in grain boundaries, which become electrically active as a result of charge trapping. The dipole moment can easily follow the changes in electric field, especially at low frequencies. Hence the contributions to dielectric constant increases through space charge polarization and rotation polarization, which occur mainly in interfaces. Therefore dielectric constant of nanostructured materials should be larger than that of conventional materials.

One of the reasons for the large dielectric constant of nanocrystalline materials at sufficiently high temperature is the increased space charge polarization due to the structure of their grain boundary interfaces. Also, at sufficiently high temperature the dielectric loss is dominated by the reason for the sharp increase of the dielectric constant at low frequencies and at lower temperatures. As temperature increases, the space charge and ion jump polarization decreases, resulting a decrease in dielectric constant.

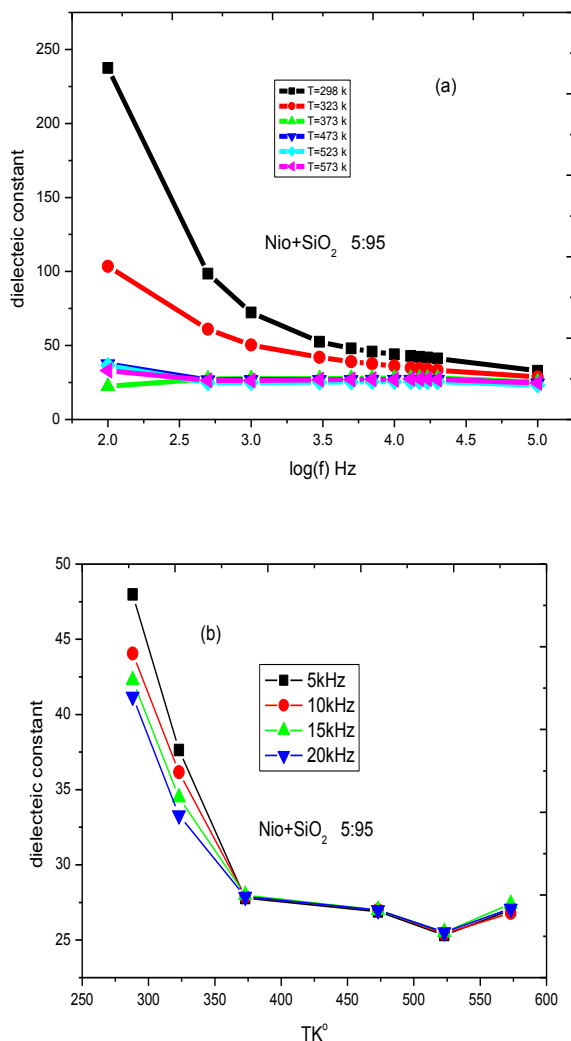


Fig. 6.(a). The frequency dependence of the dielectric constant ,
 (b) dependence the dielectric constant with temperatures for nano $(\text{SiO}_2)_{100-x}:(\text{NiO})_x(5:95)$.

3.2.3. dielectric losses

The dielectric losses calculated from the following relations[25].

where z' , ϵ' and z'' , ϵ'' are the real and imaginary parts of the impedance, dielectric constant respectively, $\tan \delta$ is the dielectric loss.

The dielectric loss factor , $\tan \delta$, for nano $(\text{SiO}_2)_{100-x}:(\text{NiO})_x$ where=5% the frequency dependence of ($\tan \delta$) at different temperatures was recorded in the range 100Hz to 100 kHz fig .7.a. show that dielectric loss decrease with fast rate at low and moderate frequency,then the decreasing rate becomes slow at high frequency region this may be attributed to the migration ion accordingly . dielectric loss at low and moderate due to the the contribution of both rings (ion jump and conduction loss) of ion migration loss , in addition to

the electron polarization loss while at high frequency values. The rest of the samples behave the same behavior representative.

Fig .7.b. the temperatures dependence of dielectric losses at constant frequency for nano (SiO₂)_{100-x}:(NiO)_x where x=5% these curves show that the dielectric losses for all sample generally decrease as the temperature increases As temperature increases, the space charge and ion jump polarization decreases, resulting a decrease in dielectric losses.

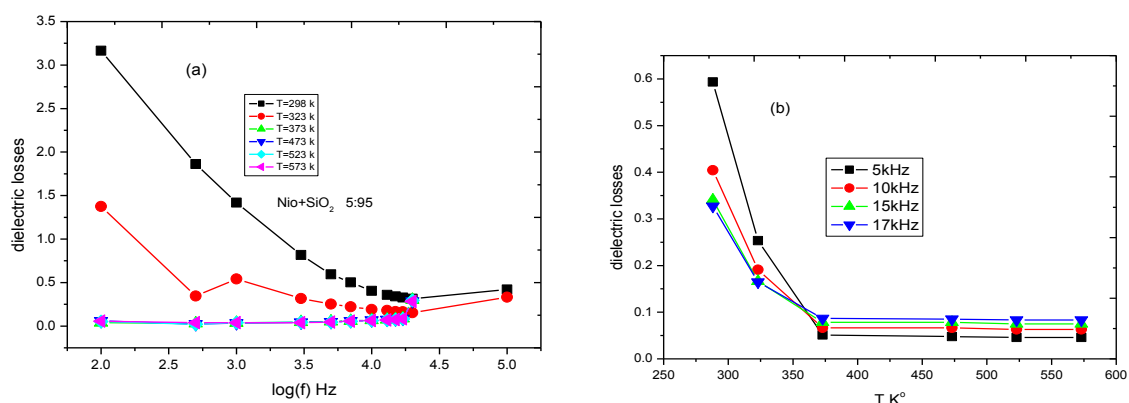


Fig. 7.(a). relation between dielectric loss, and frequency at different temperatures , (b) dependence the dielectric loss with temperatures for nano (SiO₂)_{100-x}:(NiO)_x, (5:95).

3.3. 1. Optical properties of nano (SiO₂)_{1-x} : (NiO)_x glass

UV-visible measurements

Fig.8. Optical absorption measurement gives at the room temperature absorption spectra of the nano

(SiO₂)_{1-x}: (NiO)_x glass nanocomposites. showed a broad absorption peak at the wavelength of 392 nm ,656 ,and at 714 nm The UV–vis absorption spectra of samples present the typical bands of NiO these spectra have comparatively a much lower absorption at higher wavelengths (from 700 nm) [26] . There is a change in absorption with the NiO content increases, the excitonic peak exhibits its signature. It is seen that the absorption edge corresponding to the nanocomposites gets red shifted and the exciton oscillator strength increases as a function of the NiO content consistent with published report [27]. The structure and size evolution of the nanocomposites may also have some relation with optical characteristics in addition to the composition. Note increases the absorption UV agree with the results of the absorption XRY and FTIR.

Fig .9. The direct optical band gaps were obtained from the linear plots of $(\alpha h\nu)^2$ versus $h\nu$ as shown for sample

SiO₂: NiO 70:30 the optical band gap (E_g) in a semiconductor is determined by assuming the nature of transition (n) and plotting $(\alpha h\nu)^2$ vs. $h\nu$ where n represents the nature of transition. Now, n may have different values, such as 1/2, 2, 3/2 or 3 for allowed direct, allowed indirect, forbidden direct and forbidden indirect transitions, respectively. For allowed direct transition one can plot $(\alpha h\nu)^2$ vs. $h\nu$ and extrapolate the linear portion of it to as 0.4971 value to obtain the corresponding band gap (E_g). However, for the nanocrystalline (SiO₂:NiO) composite glass it was intended not to pre-assume the nature of optical transition and determine the n values for each of the composite prepared. If (n) represents the nature of optical transition in may be

expressed as [28] .semi conducting material, the absorption coefficient (α). Also the Optical band-gap is set for each sample of 5%, 10%, 15% , 20% and 25% have similar of the values are as Table 4.

$$\alpha = (A/h\nu)(h\nu - E_g)^n$$

where α is the absorption coefficient, ν is the frequency, h is the Planck's constant, A is a constant, E_g is the optical energy band gap between the valence and the conduction bands and n is the power that characterizes the transition process.

Table 4
Activation energy E_g is determined by direct transitions for all sample nano (SiO₂)_{1-x}: (NiO)_x

Nio content wt%	Optical band-gap (E _g)(ev)
5%	0.489
10%	0.490
15%	0.495
20%	0.486
25%	0.494
30%	0.497

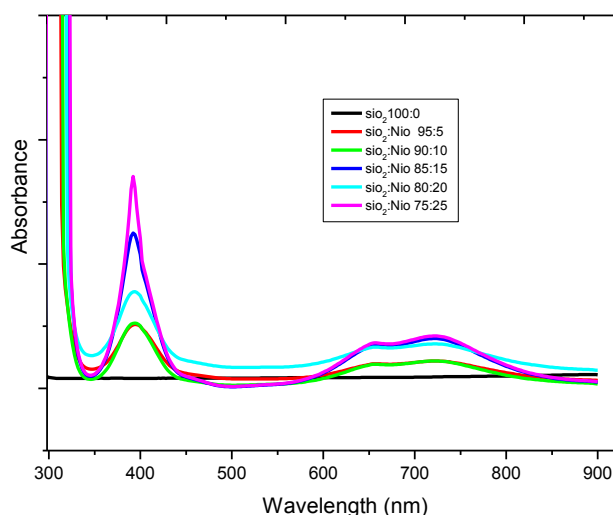


Fig. 8. Optical Absorption vs. wavelength (λ) for nano(sio₂)_{1-x}:(Nio)_x glass

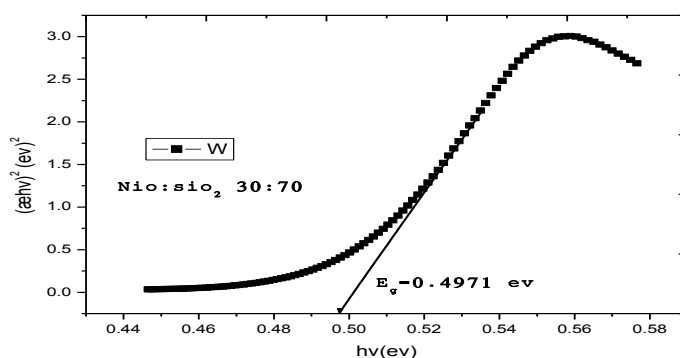


Fig. 9. The plot of $(\alpha h\nu)^2$ versus $(h\nu)$ (ev) for nano(sio₂)₇₀:(Nio)₃₀ glass .

3.4.1. Saturation magnetization and coercivity

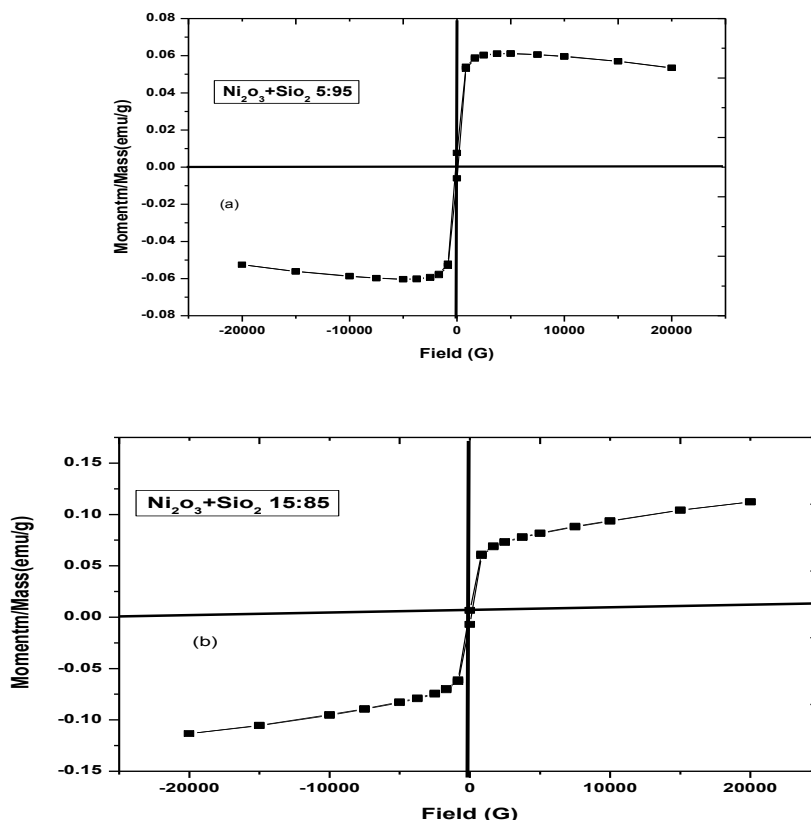


Fig.(10). The hysteresis loops ,measured at 0k of the (a) (siO₂)₉₅:(nio)₅ and (b) (siO₂)₈₅:(nio)₁₅ respectively.

The hysteresis loops are reported in fig .10. (a) for sample (SiO₂)₉₅ :(NiO)₅ and in fig 10.b) for sample (SiO₂)₈₅: (NiO)₁₅

The coercivity values H_c ,the magnetization M_s and the remanence values M_r and the reduced remanence M_r/M_s obtained from the hysteresis loops are reported in table (4). As it can be seen, the magnetic properties of the samples clearly depend on the nickel loading and the NiO particle size. It is evident from Fig. 10. that the saturation magnetization (M_s) decreases with decreasing Nio content, as expected, since this parameter depends on the total mass of the magnetic material. The reduction of this value may because by non-co linearity of the magnetic moments at the surface of the nano-particles, resulting in a decrease of the saturation magnetization for a lower Ni o content[29]. The decrease in remnant magnetization (M_r) can be attributed to a decrease of the mean size of nano-crystallites. On the other hand, the super-Paramagnetism is often observed for magnetic particles below 10 nm .One can see that the values of the saturation magnetization for Ni increase, while the coercive field values decrease, by increasing (NiO) content[30].

Table 4: Magnetic parameters of nano (SiO₂)_{100-x} : (NiO)_x glass .

Nio%	Coercivity (H _c)G	Magnetization (M _s)emu/g	Rententivity (M _r) emu/g	nano particles size(nm)	M _r /M _s
5	96.128	60.843x10 ⁻³	6.8403x10 ⁻³	5.55	0.1124
15	83.944	112.85x10 ⁻³	6.7698x10 ⁻³	4.56	0.05998

IV. Conclusions

Nickel oxide doped silica glass matrix have been successfully synthesized via sol-gel process for different percentage of NiO in the matrix. XRD patterns of the composite powder confirmed the crystalline face structured of NiO dispersed in the silica matrix and the average size of the particles can be calculated by the Scherrer formula (4.6-9.04 nm). Transmission electron microscopic images and corresponding selected area diffraction pattern confirmed the formation of NiO nanoparticles inside silica matrix. The ac conductivity, dielectric constant and complex permittivity spectrum have been studied over a wide frequency range for different percentage of NiO content in the samples. we have found. The a.c. conductivity increase with increase frequency .UV-visible measurements found the optical band gap (E_g) approx 0.49 ev. The coercivity values H_c , the magnetization M_s and the remanence values M_r and the reduced remanence M_r/M_s obtained from the hysteresis loops From these data, it was found that the saturation magnetization for NiO increases, while the coercive field values decrease, by increasing NiO content.

Reference

- [1]. S.-P. Szu, C.-Y. Lin / Materials Chemistry and Physics 82 (2003) 295–300
- [2]. A.P. Alivisatos, Science 271, 933, 1996
- [3]. D. Niznansky, N. Viart, J.L. Rehspringer, J. Sol-GelSci. Technol. 8, 615, 1997
- [4]. R. Pool, Science, 248, 1186, 1990
- [5]. A. Hasselbarth, A. Eychmuller, H. Weller, Chem. Phys.Lett. 203, 271, 1993
- [6]. NSTI-Nanotech 2004, www.nsti.org, ISBN 0-9728422-9-2 Vol. 3, 2004
- [7]. M. Raileanu et al. / Journal of Non-Crystalline Solids 354 (2008) 624–631
- [7]. C.J.Brinker and G.W.Scherer, 'Sol-gel science: the physics and chemistry of sol-gel processing' Academic press, New York, 1990.
- [9]. M. Raileanu et al Rom. Journ. Phys., Vol. 50, Nos. 5–6, P. 595–606, Bucharest, 2005.
- [8]. A. Jitianu, M. Crisan, A. Meghea, I. Ra'u, M. Zaharescu, J. Mater. Chem. 12 (2002) 1401.
- [9]. S. Roy, D. Das, C. Chakravorty, D.C. Agrawal, J. Appl. Phys. 74 (1993) 4746.
- [10]. L. Narvaez, O. Dominguez, J.R. Martinez, F. Ruiz, J. Non-Cryst. Solids 318 (2003) 37.
- [11]. G. Piccaluga, A. Corrias, G. Ennas, A. Musinu, Sol-Gel Preparation and Characterization of Metal-Silica and Metal Oxide-Silica Nanocomposites, Materials Science Foundations, Trans Tech Publications, Switzerland, 2000.
- [12]. M.A. Ermakova, D. Yu. Ermakov, S.V. Cherepanova, L.M. Plyasova, J. Phys. Chem. B 106 (2002) 11922.
- [13]. K. Takeuchi, T. Isobe, M. Senna, J. Non-Cryst. Solids 194 (1996) 58.
- [14]. Hernandez-Torres, A. Mendoza-Galvan, Thin Solid Films 472 (2005) 130.
- [17] D Buso et al/ Nanotechnology 18 (2007) 475505.
- [18]. C. Cantalini et al. / Sensors and Actuators B 108 (2005) 184–192.
- [19]. A.M.Ali,RNajmy/catalysis Today 208 (2013) 2-6.
- [20]. S.C. Tjong, H. Chen / Materials Science and Engineering R 45 (2004) 1–88.
- [21]. M. Salavati-Niasari et al. / Inorganica Chimica Acta 362 (2009) 4937–4942.
- [22]. S. Nandy et al. / Journal of Alloys and Compounds 453 (2008) 1–6.
- [21]. M.M. Elkholy, RA. El-Ma Nawany 1 Materials Chemistry and Physics 40 (1995) 163-167.
- [23]. Sevi Murugavel et al. Journal of the Indian Institute of Science VOL 91:2 Apr–Jun 2011(303-317).
- [15]. ISSN: 0973-7464 Vol. XVII: No.1 & 2 SB Academic Review 2010 : 93-100.
- [16]. S. Nandy et al. / Journal of Alloys and Compounds 453 (2008)
- [17]. M. Llusar et al. / Journal of the European Ceramic Society 29 (2009) 3319–3332
- [18]. L. Irimpan et al. / Optical Materials 31 (2008) 361–365.
- [28]. S. Chakrabarti et al. / Thin Solid Films 441 (2003) 228–237.
- [29]. Aust. J. Basic & Appl. Sci., 5(10): 287-295, 2011.
- [19]. Li, L., G. Li, R.L. Jr. Smith, H. Inomata, 2000. J.Chem. Mater. 12, 3705 (2000).Li L., Li G., Smith R.L., Inomata H., J.Chem. Mater, 12: 3705.